Earth Space Elevator Feasibility

An orbital tether reference design, materials catalog audit and siting study

Matha Labs Research · 21 November 2026 · Technical preprint 1.0

Abstract

An Earth space elevator would use a tensioned equatorial ribbon extending through geostationary orbit (GEO) to transfer uncrewed cargo. We derive a constant-allowable-stress benchmark, investigate distributed propulsion hardware, audit the public GNoME crystal release and screen terrestrial support sites and equatorial anchor regions. In a spherical equatorial Earth model, the effective work to GEO is 48.423 MJ/kg. A geometric taper of 20 requires 16.16 MJ/kg of allowable specific tensile strength. At 1,600 kg/m^3, a factor of two on ultimate strength and 60% installed strength retention imply an ultimate tensile stress of 86.2 GPa in the specified engineering product. A published 12.5 GPa carbon nanotube fiber measured 7.5 MJ/kg at laboratory gauge, implying a static taper of about 637 even before design reductions. The public GNoME audit supplies leads for follow-up calculations, and its fields do not establish qualification. The results support a stage-gated materials and climber program. The Blender reference illustrates mechanical interfaces and orbital deployment dependencies.

1 Research question and methods

Can a qualified, manufacturable tension member support an Earth-to-GEO cargo corridor at a bounded taper and deliver competitive throughput? We evaluate four constraints in sequence. First, derive a static reference with gravity, centrifugal acceleration, surface pretension and tension at the counterweight. Second, compare engineering-product tensile evidence with the resulting allowance and audit the fields available for inorganic candidates. Third, screen anchor and logistics locations against equatorial alignment and observable marine and infrastructure proxies. Fourth, compare traction and captive linear electromagnetic propulsion at an orbital systems level. Each result is conditional on the assumptions given with it. Reproduction files contain the numerical profiles, materials evidence, catalog audit and scores.

Pearson derived an exponential taper for an Earth orbital tower. Edwards considered an equatorial offshore anchor, a ribbon expanded by later climbers and space deployment from a seed tether. This study extends the same equilibrium problem with an explicit constant distributed mass penalty and keeps specimen tensile measurements separate from installed allowances. The reference uses an axisymmetric gravitational and centrifugal field with a straight, static equatorial ribbon, a spherical equatorial radius and Newtonian point-mass gravity. It excludes Earth oblateness, lunisolar and radiation pressure perturbations, atmospheric forcing, line elasticity, moving masses and orbital conjunctions. The model is an analytical lower-complexity benchmark for coupled engineering. Pearson, 1975 · Edwards, 2000 · NASA NIAC phase II.

2 Rotating equilibrium and sizing

Take the equatorial surface radius R = 6,378.137 km, gravitational parameter $\mu = 3.986004418 \times 10^{14}$ m^3/s^2 and sidereal angular speed $\omega = 7.292115 \times 10^{-5}$ rad/s. The effective inward acceleration is $g_{eff}(r) = \mu/r^2 - \omega^2 r$. GEO

occurs at r_G = (μ/ω²)^(1/3), 35,786.0 km above the equatorial surface. The integral of g_eff from R to radius r defines Φ(r), the work per unit mass against effective gravity. It rises to a maximum at GEO and falls beyond GEO. An endpoint at 100,000 km altitude is a chosen sizing case with negative effective gravity and a tip mass supplying an outward boundary force. NGA WGS 84 system.

$$\Phi(r) = \mu\,(1/R - 1/r) - (\omega^2/2)\,(r^2 - R^2)$$
$$dT/dr = g_{eff}(r)\,[\rho\,A(r) + \lambda(r)]$$
$$T = \sigma_{allow}\,A, \quad S = \sigma_{allow}/\rho$$
$$A(r)/A(R) = \exp[\Phi(r)/S] \qquad \text{when } \lambda = 0$$

Here T is tension, A is the load-bearing area, ρ is its installed bulk density, σ_allow is the allowable axial stress, S is the allowable specific tensile strength and λ is the mass per unit length of non-load-bearing hardware. The solution follows by substituting dT/dr = σ_allow dA/dr and integrating. The lower ribbon adds inward weight and raises tension as radius increases. Beyond GEO the distributed centrifugal load reduces required tension with radius. The tip equilibrium is $T_{tip} = M_{tip}[\omega^2 r_{tip} - \mu/r_{tip}^2]$. The maximum area lies at GEO in this continuous unloaded case. A GEO station idealized as a point mass exactly at GEO has zero net effective radial body force, but its mass matters to dynamics, stationkeeping, deployment and local load paths.

For constant λ, define a = λ/ρ. Then A(r) = [A(R) + a] exp[Φ(r)/S] − a. This analytic penalty captures rail, comms or protection mass carried by the ribbon. An attachment pattern that scales with local ρA by mass fraction f gives an effective exponent multiplier of 1 + f. Neither approximation captures local loads, irregular spans, stress concentrations or support transitions. Above GEO the calculation assumes sustained positive tension throughout. A design with different endpoints must verify this explicitly.

Maximum GEO to surface area ratio	Minimum allowable specific strength in MJ/kg	Required ultimate strength in GPa at 1,600 kg/m³
5	30.09	160.5
10	21.03	112.2
20	16.16	86.2
30	14.24	75.9
100	10.51	56.1

Ultimate strength column assumes σ_allow = kσ_ultimate/F, with installed retention k = 0.60 and F = 2. These are scenario inputs, not certification factors. In qualification, replace this product with a statistical allowable for the built ribbon and junctions, and explicitly account for operational load combinations. Applying the assumed factor to an already derated measurement would double-count damage.

A mass example holds surface tension at 100 kN, density at 1,600 kg/m³ and allowable stress at a hypothetical 25 GPa. It assumes no distributed hardware in the bare case. Areas are 4.00 mm² at the anchor, 88.71 mm² at GEO and 25.22 mm² at the tip. The area ratio is 22.18. Tension reaches 2.218 MN at GEO and 0.630 MN at the tip. Simpson quadrature integrates 3,471 metric tons below GEO and 6,167 above it. With 1,188 t of idealized tip mass, the structure contains about 10,826 t before adding stations, climbers and the anchor. A normalized design's installed width, thickness, number of lanes and stability limits remain open. All masses in this particular constant-stress case scale linearly with surface tension when the relative hardware mass case stays fixed.

Uniform attached mass relative to bare anchor line density	Added hardware in t	Area at GEO in mm²	Tip mass in t	Total ribbon, hardware and tip in t
0%	0	88.71	1,188	10,826
1%	6.4	89.55	1,198	10,933
10%	64	97.18	1,288	11,890
100%	640	173.42	2,188	21,464

The 100% case represents a uniform 6.4 g/m attachment and nearly doubles the ideal system mass. This calculation illustrates why a conventional continuous rail is a poor starting assumption. It excludes any station vehicle fleet, power conversion or heat rejection system. Even a single 1,000 kg climber adds a near-surface radial force of 9.76 kN, about 9.8% of the reference pretension. The model excludes that load. An optimized profile under moving traffic must include point loads, reevaluate pretension and use simultaneous radial and lateral margins.

2.1 Energy, angular momentum and dynamic loads

At 200 km/h constant radial speed, an illustrative transit reaches GEO in 7.46 days. The minimum mechanical work is 13.45 kWh per gross kilogram. A uniform 75% electrical-to-mechanical efficiency raises input to 17.93 kWh/kg before transmission, environmental and hotel loads. A 1,000 kg gross vehicle draws about 723 kW at the surface on this model. Peak power occurs in the strongest effective gravity and falls with altitude. The corresponding inertial specific energy increase is 57.66 MJ/kg, including 9.24 MJ/kg of work exchanged through torque with Earth's rotation. This follows from $\Delta E_{inertial} = \Phi + \omega \Delta \ell$, where $\ell = \omega r^2$ is specific axial angular momentum. Recoverable descending energy depends on traffic matching, electrical routing, fleet mass and conversion losses.

The rotating frame produces tangential Coriolis acceleration $2\omega v_r$ with sign reversed between ascent and descent. A constant 200 km/h 1,000 kg ascent requires about 8.10 N of local tangential guide force from this term alone. Over days the distributed response matters more than an isolated contact force suggests. Multiple moving loads, resonance, wind and imposed stationkeeping must be simulated together. Analyze a spatially varying string with tension T(r), line density and damping, flexible terminal boundaries, coupled radial and transverse states, and moving contact forces. Resolve lower atmospheric drag and wind on a three-dimensional ribbon. Validate mode frequencies against reduced cases, then measure drive-induced disturbances on a scaled tensioned line. Climber transit dynamics · Climber frequency optimization.

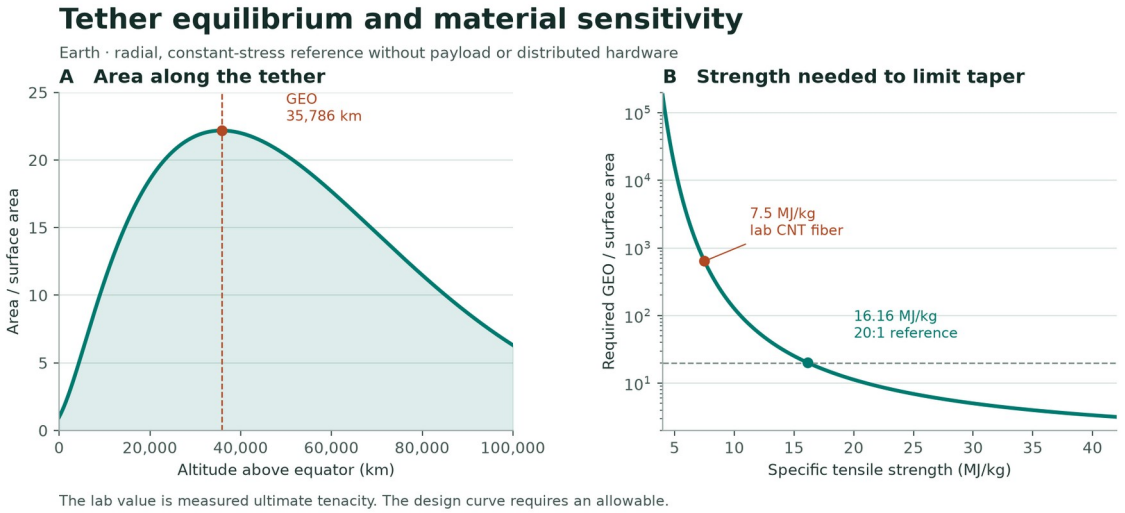

Figure 1. A. Normalized bare area over the full reference length. B. Required taper for an assigned allowable specific tensile strength. The 7.5 MJ/kg point treats the short-gauge CNT result as an allowable for illustration. Actual installed allowance would require measured retention and a design margin.

3 Materials and tensile evidence

The primary ribbon requires an aged, assembled specific allowable strength measured for the complete load path. Its numerator is the longitudinal working stress after accounting for the lower tail of the production distribution, transfer through joints and clamps, exposure, sustained loading and damage. Its denominator includes tensile fibers plus the dead mass of binders, coating, conductors and other attached systems. For a segment, the most direct measurement is tensile force divided by the as-installed linear mass. A tenacity of 1 N/tex equals 1 MJ/kg. This lets the study compare results even when porous yarns or atomically thin membranes have ambiguous cross-sectional areas.

At the best measured CNT tenacity of 7.5 MJ/kg, a factor of two alone raises the idealized taper from 637:1 to about 405,000:1. A tenacity that qualifies as an allowable after full-scale aging, manufacturing and damage reductions must be established experimentally.

Candidate and specimen	Tensile strength	Density	Ultimate specific strength	Evidence and interpretation
Dyneema SK99 UHMWPE fiber	≈4.12 GPa derived	0.97 g/cm^3	4.25 MJ/kg	Combines 42.5 cN/dtex from the manufacturer with the reported density of an SK99 specimen used in separate research. Use as a terrestrial reference and qualify creep and terminations. Dyneema · SK99 specimen density
Toray T1100G PAN carbon fiber	7.0 GPa	1.79 g/cm^3	3.91 MJ/kg	Manufacturer fiber data from the impregnated-strand method. Laminate, bend and termination values require separate tests. Toray
Toyobo Zylon HM PBO fiber	5.8 GPa	1.56 g/cm^3	3.72 MJ/kg	Manufacturer fiber data. Separate NIST yarn aging experiments show strong sensitivity to combined heat and moisture. Toyobo · NIST aging study
Kuraray Vectran HT yarn	3.40 GPa derived	1.40 g/cm^3	2.43 MJ/kg	Manufacturer reports 24.3 cN/dtex for a 1,670 dtex yarn with its own test method. Kuraray

Candidate and specimen	Tensile strength	Density	Ultimate specific strength	Evidence and interpretation
DuPont Kevlar 49 yarn	3.00 GPa	1.44 g/cm³	2.08 MJ/kg	Manufacturer conditioned-yarn typical. The same guide gives 3.60 GPa in the resin-impregnated strand test, illustrating the sensitivity to specimen form and procedure. DuPont
Aligned and densified CNT fiber	12.5 GPa	1.67 g/cm³ implied	7.5 MJ/kg	Wang et al. report the best-case strength and tenacity. The gauge study covered 2–50 mm and showed some reduction at 40–50 mm. The 75 cm rope demonstration carries a separate hanging load and establishes no equivalent rope-level breaking stress. Wang et al., 2026
Hierarchical CNT fiber	8.2 GPa quasi-static, 14 GPa dynamic	—	—	The 14 GPa result applies to high strain rate. Quasi-static and stress-rupture data govern sustained tether loads. Science, 2024 · CAS
Wet-spun graphene fiber	5.9 GPa	—	—	Measured macroscopic fiber and 963 GPa Young modulus reported. Assembly defects and transfers between layers govern scale-up. Liu et al., 2026
Laboratory ultralong CNT bundle	>80 GPa	—	—	Direct measurements on specialized centimetre-long bundles of ultralong nanotubes. Bundle geometry, solid area and production route differ from an engineered tether. Bai et al., 2018
Defect-free graphene monolayer	~130 GPa equivalent	—	—	The measured intrinsic breaking load per width was 42 N/m by nanoindentation. The stress value uses a conventional monolayer thickness. An assembled fiber requires independently measured load and mass. Lee et al., 2008
Ideal diamond nanothread	15.7 nN force	—	up to 26 MJ/kg	First-principles prediction for an isolated thread configuration. Physically synthesized nanothread bundles establish a building block with short-range axial order. DFT study · Fitzgibbons et al., 2015
Ideal carbyne chain	~10 nN force	—	up to 75 MJ/kg	First-principles prediction for an atomic carbon chain. Experiments produced long carbon chains inside double-walled nanotubes. Host mass, stabilization and continuous load transfer remain open. Liu et al., 2013 · Shi et al., 2016

Prototype materials can be specified regionally with commercial grades. ASTM A572 Grade 50 plate has 345 MPa minimum yield and 448 MPa minimum ultimate strength (50 and 65 ksi). It is a reference stock for a dry structural base or test load frame. An actual ocean platform would require marine-class scantlings, vessel fatigue design, corrosion protection and qualified welds. Hydro 6061-T6 extrusion has 240 MPa minimum yield and 260 MPa minimum ultimate strength in the tabulated product form. This is reference material for a dry climber frame, with weld heat-affected zones and buckling governing assembly sizing. Titanium Grade 5 plate has 828 MPa minimum yield and 895 MPa minimum ultimate, at 4.43 g/cm³. It is a candidate for local clamp/load-transfer hardware where bearing strength, galvanic isolation and wear matter. C11000 copper serves electrical windings and busbars by conductivity and temper. For any cabin, space-facing coating or dielectric, process and tested part geometry determine suitability. These values identify source stock and do not substantiate prototype capacity. AISC plate data · Hydro 6061 · ATI 6-4 · Copper Development Association

3.1 Google DeepMind GNoME catalog audit

Merchant et al. used graph neural networks and active learning to propose inorganic crystal structures and density functional theory to evaluate their energies. Their 2023 paper reports approximately 2.2 million structures calculated below the prior convex hull and approximately 381,000 new entries on its updated convex hull. A point on a given convex hull is competitive with the available decomposition products under that calculation and reference set. The released structures and associated files have been revised since the paper. The discovery set covers the candidates generated under the project's search and data rules. Commercial fibers are assembled or polymeric forms whose performance depends on microstructure and geometry beyond a periodic unit cell. Merchant et al., 2023 · DeepMind dataset versioning and schema

We parsed both complete public CSVs from pinned Cloud Storage generations and validated file hashes before reading any records. The December 2024 summary comprises 554,054 distinct material IDs with 554,054 distinct reported reduced formulas. Its Cheon topology field gives 1,685 entries tagged 1D and 4,069 tagged 2D, while 68,784 lack a tag. The companion has 139,541 distinct r²SCAN records, 117,043 of which join to IDs in the newer summary. The release provides chemistry, density, cell volume, lattice symmetry, computed energies and selected other fields. Both schemas lack tensile or fracture properties, elastic tensors, and manufacturing or durability tests. Some records have a missing topology, making any topology-based exclusion incomplete. The documentation labels the Density column Å³/atom. Across nine selected cases the values agreed with independent composition mass divided by cell volume in g/cm³ to within 0.0004 g/cm³. GNoME summary · GNoME r²SCAN companion · Cheon et al., 2017

An exploratory queue used the reported density at or below 2.50 g/cm³ and a 1D or 2D Cheon tag. That filter yielded 117 records, comprising 64 tagged 1D and 53 tagged 2D. Of 15 queue entries with joined r²SCAN data, six report zero in the all-entry hull field. The stricter chemistry check permitted only H, B, C, N, O and Si. Exactly three summary entries used only these elements, all tagged 3D. This illustrates the narrow coverage of lightweight chemistry in this specific release and the limited value of a geometry filter. Higher-density and 3D crystals remain possible secondary research targets. Low density and low-dimensional bonding can motivate calculations, but establish neither strong axial bonds nor weak-plane damage tolerance. Zero records supplied the mechanical evidence needed to qualify a primary tether. GNoME public dataset

A second-stage screen would recover candidate structures by ID, deduplicate against current external reference phases, and rerun the stability and dynamical checks for each production hypothesis. Directional elastic tensors could identify weak modes and stiffness anisotropy. Relaxed strain-to-failure calculations along the proposed fiber axis would then set an ideal upper bound, including phonon instabilities, stress convention, temperature, and thickness or area convention for low-dimensional systems. Explicit defect, edge and interface simulations would inform sample design. This sequence separates near-equilibrium stiffness from fracture and separates defect-free calculations from production allowables. The GNoME database is released under CC BY-NC 4.0. Materials Project elastic methodology · de Jong et al., 2015 · Google DeepMind data license

3.2 Tether qualification

An aligned CNT fiber is the leading test material in this evidence set. Its probable advantage is lower dead mass per unit tensile capacity. The governing loss mechanisms include the ends of short nanotubes, bundle pull-out, weak inter-bundle shear and local density or alignment differences. Graphene fibers face analogous sheet-overlap and interlaminar slip mechanisms. Commercial carbon fiber, aramid and LCP provide baselines for material characterization and demonstrator retention. The corresponding flight decision depends on the

surviving capacity of the ribbon laminate, a spliced and terminated ribbon and a full climb/repair load case. Wang et al., 2026 · Liu et al., 2026 · Pugno, 2007

- **Measure the distributions at increasing length.** Establish failure force, linear density, modulus, strain at break and failure mode across multiple batches and gauge lengths. Progress from coupons to meter-scale strands, then to multi-lane ribbon and spliced specimens. Fit a weakest-link survival model where justified. For a single path with identically distributed independent links, an illustrative survival law is $P = \exp[-(L/L_0)(\sigma/\sigma_0)^m]$. Fit the slope from data. A multi-lane ribbon needs a separate correlated-damage and load-redistribution model.
- **Measure strength retention and load transfer.** Test scarf or staggered overlap joints, termination hardware and neighboring lanes during simulated breaks. Use force-per-width or force-per-linear-mass data for the tested assembly. Establish stress-rupture curves, creep strain, tension–tension fatigue, pinch/roller abrasion, damaged residual strength and repeatability of repair. A valid joint must retain a specified fraction of the adjacent ribbon strength while distributing load with manageable strain gradients.
- **Validate the installed environment.** Condition and test specimens under relevant salt/moisture and ultraviolet exposure, thermal cycling, vacuum and outgassing, low Earth orbit atomic oxygen, charged-particle exposure and debris impact. Measure coating mass, crack growth, defects at pinholes and masked/unmasked strength separately. Use ASTM D4018 for relevant carbon-fiber tow controls, ASTM D3039/D3039M for appropriate polymer-matrix coupons, and an explicit additional tether test plan for long splices and whole assemblies. ASTM composite standards · NASA materials standard · NASA atomic oxygen durability handbook

The main release gate is a statistically supported end-of-life specific allowable for the installed primary ribbon consistent with the selected taper and dynamic load case. Splice reliability, continuous quality assurance, production yield, replacement rate and survival after lane loss are independent pass conditions. A later program can derive sample sizes and failure probabilities from the target service reliability and the observed distributions. The current data justify materials experiments and a prototype climber program. Fabrication of an Earth-to-GEO ribbon remains gated by the results of those experiments.

4 Equatorial anchor and logistics siting

A conventional Earth elevator occupies the rotational equatorial plane. A free geostationary node must hold a fixed longitude in that plane. At offset z along the rotation axis, the centrifugal acceleration has zero z-component, while gravitational acceleration contributes $-\mu z/r^3$. An off-equator ground terminal would therefore require a different architecture with a curved tether and a separately demonstrated cross-track force balance. No U.S. landfall lies on the equator. Two sample positions in the U.S. exclusive economic zone (EEZ) around Howland and Baker Islands are worth a federal desk review. A separate offshore corridor in the eastern Pacific is the leading reference for an international study. Edwards, NIAC Phase I · Kuzuno et al., nonequatorial tether dynamics · NOAA Office of Coast Survey

Geospatial method

We sampled 23 international study positions, two U.S. EEZ study positions and one U.S. conservation comparator on the equator. The international positions span the Pacific, Indian and Atlantic oceans. A site qualifies for the offshore ranking if its median water depth is positive and its approximate distance to a mapped shore vertex is at least 200 km. The 200 km value is an explicit desk-study screen for local coastal exposure. An actual tether-break footprint could exceed it by orders of magnitude. Sixteen international positions pass. Distances use a spherical Earth radius of 6,371.0088 km and the Natural Earth 1:10 million coastline and minor-island layers. Water depths

are medians from two gridded latitude rows at approximately ±0.00833° and nearby longitude cells within 0.05° of each point. Marine Regions EEZ polygons provide a point lookup for preliminary water-column jurisdiction. They do not identify every protected area, shelf claim, or use restriction. Natural Earth coastline and minor islands · NOAA ETOPO 2022 · Flanders Marine Institute EEZ v12

For each eligible position, the baseline score equals 100 × [1 − 0.45φ(P/5) − 0.10φ(U/8) − 0.15φ(D/6000) − 0.30φ(L/5000)], where φ(x) = min(x, 1), P is corrected annual mean rainfall in mm/day, U is mean 10 m wind speed in m/s, D is water depth in meters, and L is great-circle distance in kilometers to the nearest NGA World Port Index medium or large harbor listed with at least moderate repair capacity. The rainfall and wind means come from the NASA POWER MERRA-2 January 2001–December 2025 climatology. Lower rainfall favors surface operations in this simple model. It does not measure lightning strike probability. Depth is a proxy for the complexity of surveying and any seabed infrastructure. The score does not assume the tether is tied to the seabed. Route length, berth availability, towing requirements and a port's ability to handle the eventual vessel remain open. NASA POWER climatology API · MERRA-2 data documentation · NGA World Port Index · U.S. DOE port-data mirror

Cyclone exposure was checked separately against 293,940 published center positions from 4,683 IBTrACS primary tracks, 1981 through 2025. This calculation counts distinct systems whose sampled centers came within 250 or 500 km. It does not measure storm swells, the wind field outside the track, future changes or near-equator squalls. The eastern Pacific reference had zero sampled centers within 500 km. The western Indian Ocean reference had two, and the Phoenix Islands sector one. The U.S. Howland–Baker sites had one system each within 250 km and three and six within 500 km, respectively. The historical nearest sample at the western U.S. position was about 46 km away. Knapp et al., 2010 · NOAA IBTrACS v04r01

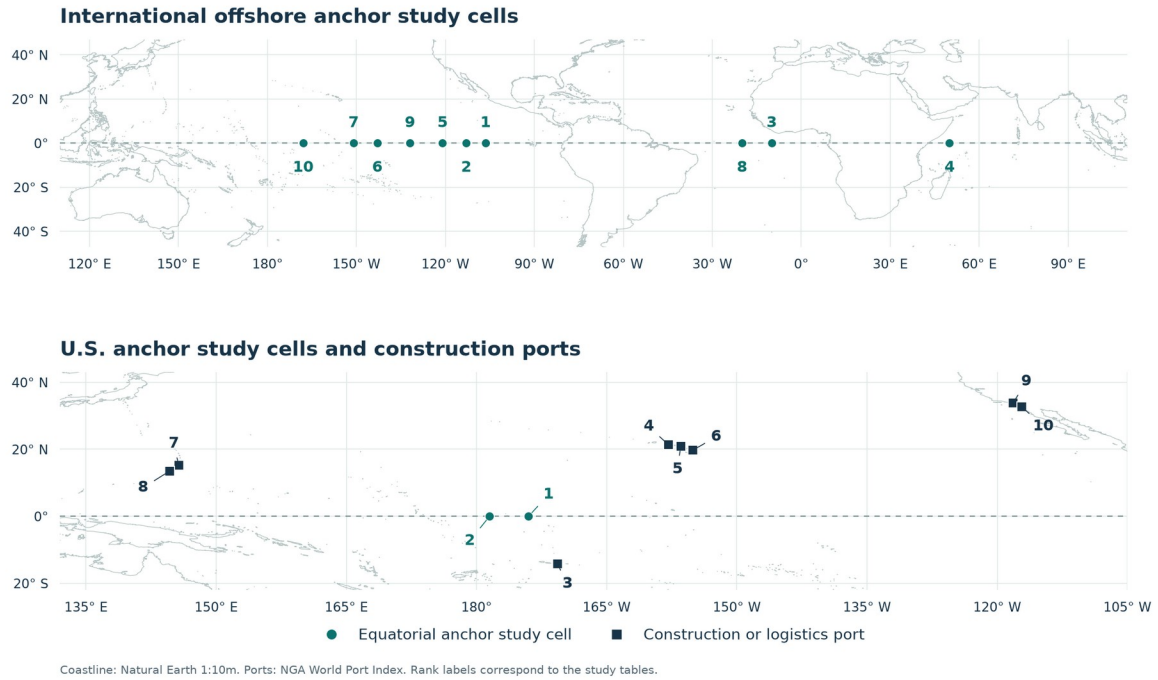

Figure 2. International equatorial anchor study cells and the United States anchor and support-port network. Rank labels match the two tables. The positions are screening hypotheses and the map uses Natural Earth shorelines.

United States sites

The first two rows are equatorial anchor survey cells in the same U.S. EEZ. The other eight are real U.S. buildout or support ports ordered by straight-line distance to the nearer proposed U.S. anchor. The rows do not imply ten available anchor sites.

Rank	Location	Latitude, longitude	Role and main constraint
1	Howland–Baker east	0°, 174.00° W	Anchor study. 5,389 m depth, 274 km from mapped shore, 2.21 mm/day rain.
2	Howland–Baker west	0°, 178.50° W	Anchor study. 5,400 m depth, 225 km from mapped shore, 2.76 mm/day rain.
3	Pago Pago, American Samoa	14.28° S, 170.67° W	1,630 km. Forward stores and crew transfer. The World Port Index lists limited repair.
4	Honolulu, Hawaii	21.30° N, 157.87° W	2,946 km. Regional repair and resupply. Confirm dry-dock dimensions and berth availability.
5	Kahului, Hawaii	20.90° N, 156.47° W	3,005 km. Secondary crew staging and stores at a very small indexed harbor.
6	Hilo, Hawaii	19.73° N, 155.07° W	3,011 km. Resupply and moderate indexed repair.
7	Saipan, Northern Mariana Islands	15.20° N, 145.68° E	4,282 km. Western logistics backup. The index lists no repairs.
8	Apra Harbor, Guam	13.45° N, 144.62° E	4,329 km. Western Pacific cargo and engineering support. The index lists limited repair.
9	Long Beach, California	33.77° N, 118.18° W	6,911 km. Mainland cargo consolidation and major indexed repair.
10	San Diego, California	32.72° N, 117.18° W	6,959 km. Mainland integration and major indexed repair.

The two U.S. survey positions lie beyond the published Howland–Baker monument boundary at their longitudes. The eastern monument limit is 175°38′32″ W and the western limit is 177°27′07″ W. An EEZ conveys specified coastal-state rights and jurisdiction. The two cells are beyond the territorial sea and lack installation authorization. Jarvis provides another U.S. equatorial EEZ intersection, but the Jarvis monument extends to its EEZ outer limit and the island refuge has restricted access. The study excluded the Jarvis comparator at 160.85° W. Openings for particular fishing activities have no bearing on the assumed availability of a tether installation. The Federated States of Micronesia, the Marshall Islands and Palau are sovereign nations with U.S. Compacts of Free Association. Their ports and waters require distinct host-state engagement. USFWS official monument description · USFWS published monument limits · USFWS Jarvis refuge · U.S. Department of the Interior compacts

International offshore alternatives

Coordinates denote the centers of study areas on 0° latitude. All ten shortlisted positions fall outside the EEZ polygons queried in Marine Regions. A location name refers to a broad geographic sector. It does not imply territorial control by nearby islands. The weather columns report means, and the port column shows a distance proxy.

Rank	Sector and longitude	Depth (m)	Rain (mm/day)	Wind (m/s)	WPI port (km)	Score
1	Eastern Pacific reference, 106.5° W	3,729	0.47	4.80	Manzanillo, 2,132	67.7
2	Eastern Pacific west, 113° W	4,063	0.45	5.06	Manzanillo, 2,320	65.5
3	Central Atlantic east, 10° W	5,006	1.22	4.79	Abidjan, 884	65.2
4	West Indian Ocean, 50° E	5,080	1.14	5.43	Mombasa, 1,234	62.8
5	East-central Pacific east, 121° W	4,332	0.46	5.44	Manzanillo, 2,793	61.5
6	East-central Pacific west, 143° W	4,396	0.55	6.03	Hilo, 2,558	61.2
7	Line Islands east, 151° W	4,322	0.84	6.04	Hilo, 2,239	60.7
8	Central Atlantic central, 20° W	2,712	1.83	5.05	Dakar, 1,657	60.5
9	East-central Pacific central, 132° W	4,362	0.48	5.82	Hilo, 3,336	57.5
10	Phoenix Islands sector, 168° W	5,246	1.76	5.75	Hilo, 2,608	48.2

The eastern Pacific reference at 106.5° W led the baseline and weather-led cases. The weather-led weights were 60/15/10/15 percent for rainfall, wind, depth and access. Increasing the access weight to 55 percent with 25/5/15 percent for the other terms moves 10° W to first and 106.5° W to fourth. At 300 km from shore the ten-site order stays the same. At 100 km the 81.75° W cell off Ecuador enters first, supported by 1,246 m estimated water depth and a 1,024 km repair-port distance. The reference therefore explicitly excludes a highly ranked nearshore alternative on a coast with a documented subduction and tsunami hazard. Each set of scores ranks the sampled positions rather than every longitude or every authorized siting option. USGS 2016 Ecuador earthquake and regional tectonics

Site qualification and governance

Advance the eastern Pacific, central Atlantic and Howland–Baker east cells to comparative desktop studies. Make a narrower decision only after site-specific joint wind, current, and sea-state return values and seasonal availability are estimated, including multi-year ENSO variability. Sample measured lightning and extreme gusts alongside ambient electric field and attachment-radius modeling. Map marine mammals, fisheries, coral and other protected areas from the current conservation database and holder records. Overlay AIS, vessel routes, submarine cables, seabed rights and flight traffic with the entire platform excursion and modeled tether-failure envelope. Test vessel redundancy, port compatibility, medical evacuation and rescue times in the real service network. No shutdown or evacuation plan follows from the climatology alone. NASA LIS/OTD lightning climatology · Protected Planet, WDPCA · Global Fishing Watch satellite mapping study

Host-state authorities control whether relevant EEZ installations may be constructed and operated. UNCLOS Article 60 generally limits the safety zones it describes to 500 m unless the specified exceptions apply and bars interference with recognized sea lanes essential to international navigation. A project needs an explicit, multi-authority maritime and civil aviation plan for the full failure footprint. High-seas operation entails due regard for other lawful uses, and water-column status does not settle continental-shelf rights. The BBNJ Agreement entered into force on January 17, 2026 and provides an environmental impact assessment framework for its parties. The legal classification of each space component and its release, operation and registration warrants early consultation with the relevant states and agencies under applicable national law and international space treaties.

UNCLOS Articles 56 and 60 · UNCLOS Articles 87–89 · UN BBNJ Agreement · UN Outer Space Treaty · UN Liability Convention

5 Captive electromagnetic propulsion

A linear motor can apply continuous force to a captive car through a moving magnetic field. A ground-mounted, segmented linear synchronous motor is an engineering concept for the short rigid terminal transfer stage. The active equipment stays at an accessible atmospheric installation, with a passive carriage interface, guided travel, independent mechanical holding, position feedback and thermal monitoring. It can be demonstrated on an instrumented terrestrial rig. TK Elevator's MULTI building test demonstrates the civil architecture class. A flexible orbital ribbon adds alignment, vibration and environmental challenges that a rigid shaft does not exercise. TK Elevator MULTI.

Architecture	Load and power path	Failure behavior to verify	Reference disposition
Electrically driven traction on ribbon	Motor and converter ride with car. Verified grip directs shear into ribbon	Independent arrest, abrasion, heat and wet/salt-contaminated grip	Orbital baseline
Linear synchronous drive on rigid terminal	Fixed local stator reacts into terminal frame. Dedicated guided carriage transfers payload	Power dropout, positive capture, misalignment and handover	Ground benchmark
Car-mounted linear motor with passive orbital reaction strip	Distributed reaction material flexes with the ribbon. Car needs electrical supply and gap control	Strip fatigue/delamination, gap loss, thermal losses, fallback on bare ribbon	Research after mass and gap tests
Full-length active linear drive	Stator, electrical supply and service hardware are supported along the line	Distributed fault isolation, repair, radiation and lightning transients	Low-priority research under the mass study

The electromagnetic alternative studied here is a guided linear motor for controlled and reversible transport. Its transfer interfaces keep cargo mechanically captive along both the terminal and orbital stages. The orbital car advances on the energy budget in Section 2.1 independently of drive mechanism. It needs a credible power link. Contactless external power, local storage and staged power reception should be compared on power per installed mass, interruption duration, heat disposal and maintenance. No link or thermal design is closed here. Independent arrest must remain effective on power loss and under the permitted load envelope, including during transitions and rescue.

6 Architecture and interface assembly

The Blender package has separate orbital and local geometric scales. Hardware views illustrate functional interfaces, material choices and installation order. Orbital lengths correspond to the reference case. Ribbon width and tension scale in the visuals are exaggerated for legibility, and hardware envelopes are visual proxies. Model dimensions specify the visualization. Procurement, joints and operational hardware require the qualification evidence below. Do not sum visual model dimensions with analytical cross-sections.

Assembly	Proposed material classes	Mechanical and service interface	Acceptance evidence
Offshore terminal and load frame	Marine structural steel, corrosion protection, concrete/steel ballast	Reaction frame to platform and stationkeeping. Tension sensing at ribbon head	Structural and hydrodynamic models, storm limits, corrosion, marine assurance

Assembly	Proposed material classes	Mechanical and service interface	Acceptance evidence
Tension head and replaceable fairlead	Titanium or corrosion-resistant steel load frame. Ceramic or polymer sacrificial wear surface	Spread axial contact and allow monitored articulation	Proof load, contact pressure, minimum bend radii and retained ribbon strength
Seed and reinforced ribbons	Hypothetical aligned CNT or comparable carbon architecture. Lightweight coatings selected by altitude	Continuous primary load paths. Staggered redundant overlap transfer where validated	Long-gauge lower-tail allowance, mass per meter, fatigue and aging, and an alternate load path across damage
Splice cassette	Load-transfer laminate compatible with original ribbon, local stiffener and sensors	Develop axial load over long overlap without cutting every load path at one station	Shear transfer, post-fatigue efficiency, flaw tolerance and roller pass-through
Cargo car	Aluminum alloy/composite secondary structure, hardened wear hardware, titanium or steel fasteners	Opposed traction modules and separate capture brake. Modular sealed payload pod	Modeled contact limits, fail-safe hold, retrieval attachment and thermal test
Electromagnetic terminal cassette	Copper windings, laminated magnetic circuit, fixed structural frame and insulated feed	Short independent guideway feeds transfer cradle. Load bypasses the orbital ribbon	Force efficiency, positive capture, fault stop and repeatable mechanical handover
GEO hub	Aluminum alloy/composite truss, shielded electronics, structural hardpoints	Opposed lower and upper line interfaces. Berth loads enter the hub independently	Coupled orbit stationkeeping and redundant load path proof
Upper ribbon and tip	Same family of qualified load-bearing ribbon. Modular inert ballast and trim hardware	Ballast attaches through a monitored termination. Tip force responds to radius and trim	Positive minimum tension over perturbed operating envelope and loss of trim tests
Inspection and command	Optical strain sensors or equivalent, cameras and independent safety telemetry	Climber-based nondestructive inspection, localized environment sensors and independent arrest sensors	Fault detection with known flaws, drift, bandwidth and safe response latency

Stage A. Make line-strength and density measurements at specimen, yarn, tape and multi-lane ribbon scales with registered cross-section, gauge length and strain rate. Establish joint allowances before choosing a layup. Test representative production lengths with the oldest accepted batch, attachment treatments and environment exposures. Every assembly needs a complete mass statement.

Stage B. Qualify the terrestrial handling path. Install the marine reaction frame and articulation mock-up, then tension and instrument a sacrificial line. Commission the captive linear motor and fixed guideway. Verify controlled handover between the terminal carriage and orbital-car mock-up, including a powerless arrest and retrieval. Exercise roller wear, joint traversal, jam recovery and measurement drift.

Stage C. Validate orbital deployment in simulation and with an independently authorized short tether mission. Assemble the GEO deployment bus, spools, opposing deployment interfaces and counterweight modules. Use closed-loop tension and orbital control while deploying lines inward and outward. Starting with a GEO station does not ensure it stays geostationary as line mass moves. Control compensates for effective force, gravity-gradient modes, geometry disturbances and construction logistics. Treat the anchor as mobile for the reference architecture until capture analysis establishes the feasible motion envelope. Deployment stationkeeping study · Partially deployed elevator dynamics.

Stage D. Capture the lower ribbon only after independent dynamic validation, authorization, weather and conjunction screening, acceptable relative motion and verified positive tension. Transfer the load from the deployment capture fixture to the redundant terminal load path under monitored conditions. Inspect the continuous tether and test constrained initial operation remotely.

Stage E. Expand capacity incrementally using autonomous installation and inspection systems. Verify the load redistribution after each reinforcement run and maintain traffic separation until the modal response, braking and rescue systems are demonstrated. The conceptual seed deployment yields a different section and orbital mass balance from the steady-state mass illustration in Section 2. A separate construction-phase optimization and logistical campaign are necessary.

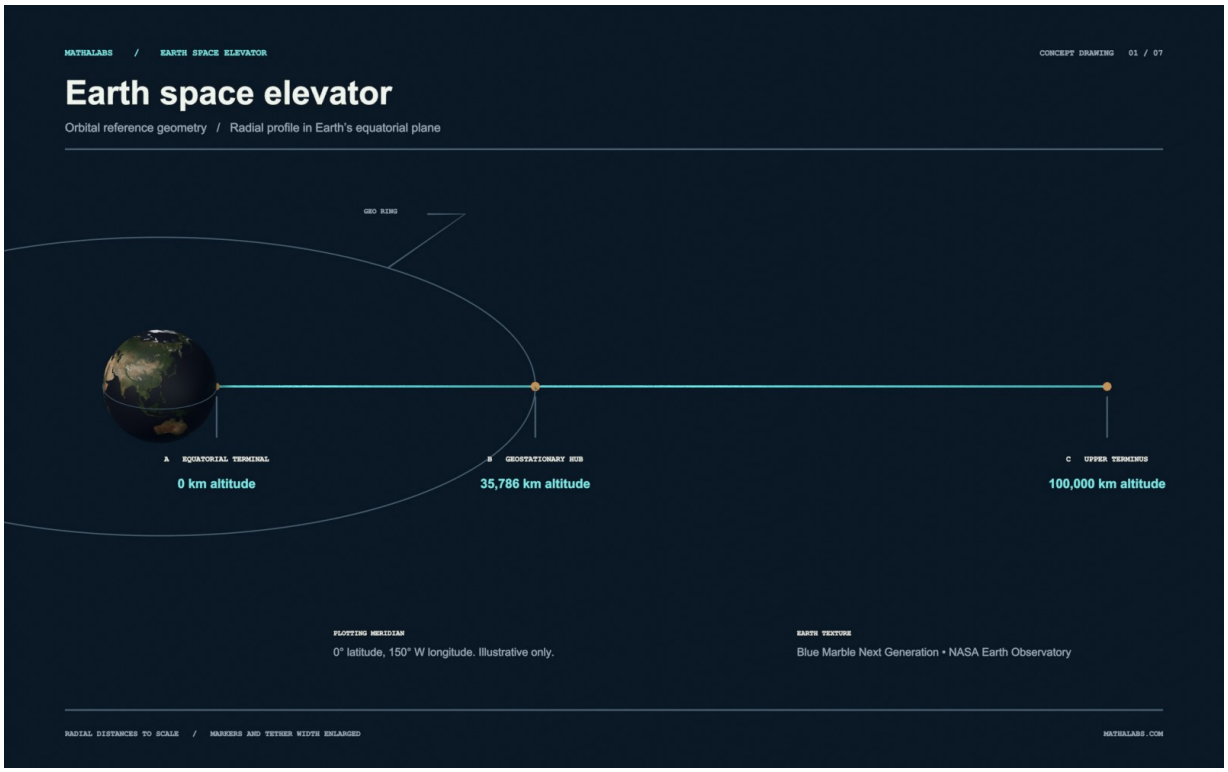

Figure 3. Orbital architecture. Geocentric distances are shown in the orbital scene. Ribbon widths and hardware markers are exaggerated. The mapped longitude is a visual datum.

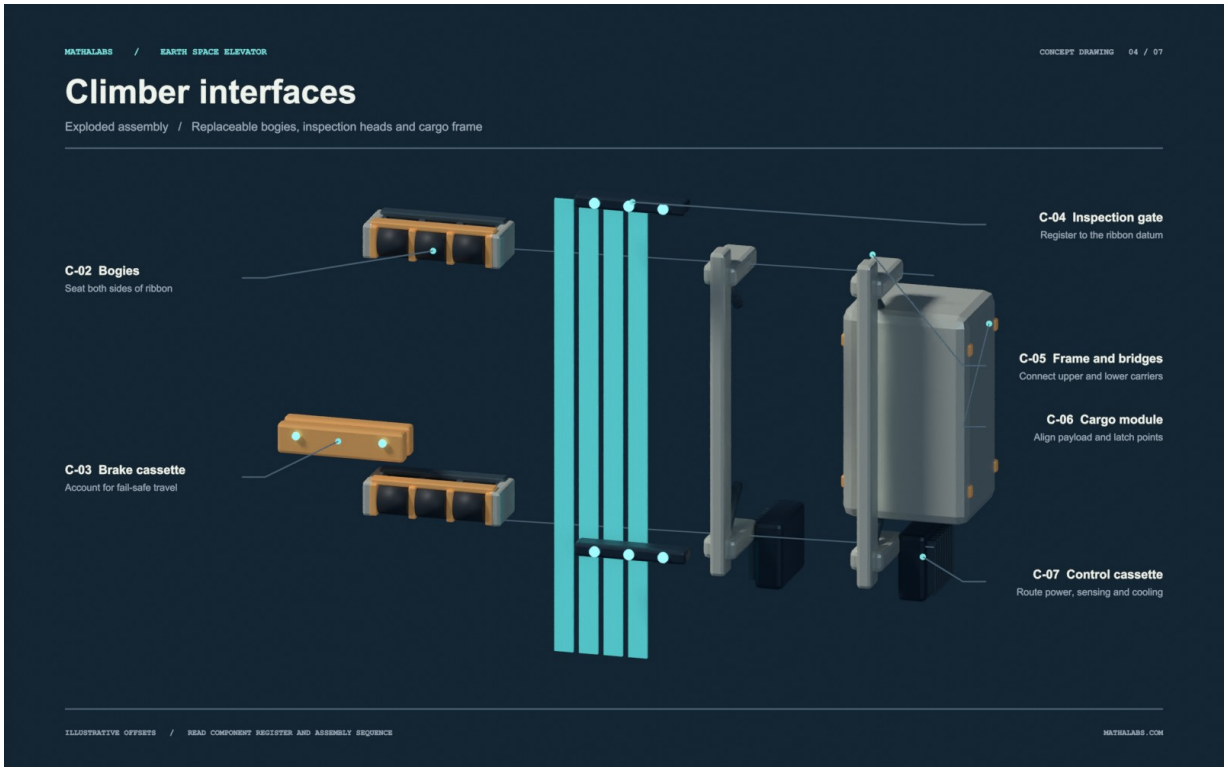

Figure 4. Exploded traction climber. Opposed bogies, independent capture hardware, structure and control cassettes are editable geometry. The model includes separate assembly and captive motor views.



Figure 5. Conceptual staggered load transfer across ribbon lanes. The witness coupon enables separate measurements of retained tensile strength and fatigue. The overlaps shown identify interfaces, while their geometry and processing require test evidence.

7 Qualification and risk gates

A deployment decision demands the lower statistical tolerance bound for retained allowable specific strength across representative batches, environments, splice states and production lengths. A series weakest-link sensitivity under independent lengths gives survival proportional to $\exp[-(L/L_0)(\sigma/\sigma_0)^m]$, where m is the Weibull shape. At fixed survival the characteristic stress falls as $(L/L_0)^{(-1/m)}$. As an illustration, scaling an independent 1 m test to 10^8 m would retain 40% for m = 20. A multi-lane ribbon with load redistribution and correlated manufacturing defects violates the independent series assumption. Infer its statistical law from hierarchical measured data and prove fail-safe load redistribution on flawed and damaged representative sections. Tensile tests need traceable area and density definitions, controls for strain rate and grip effects, plus reports on sample count and scatter.

Closure item	Decision evidence
Structural materials	Multi-lot ribbon and junction tests at multiple gauges. Retained specific strength meets a chosen taper target under aged, damaged and loaded conditions.
Atmosphere and orbital environment	Aeroelastic lifetime, lightning and current paths, salt and UV exposure, LEO atomic oxygen, radiation, thermal cycling, charging and vacuum material compatibility.
Collision and line continuity	Altitude-resolved flux and crossing probabilities, conjunction data for trackable objects, puncture and progressive tear tests, repair coverage and independent risk analysis for failure.
Dynamics and operations	Elastic three-dimensional models anchored to tests, storm and platform motion envelope, moving climber and construction cases, safe stop without cascading loss of tension.
Governance and terminal siting	Host jurisdiction and international coordination, enforceable risk and liability allocation, air/marine traffic plans, fisheries and environmental evidence, emergency response and community consultation.
Energy and economics	Verified climber mass fraction, power delivery and heat management across altitude, fleet and maintenance simulation, demand and schedule with financing and replacement costs.

NASA's ORDEM supplies directional debris flux estimates to GEO under its modeled regimes. Estimate expected impacts by integrating the directional relative flux times projected ribbon area over altitude, orientation and service time. Use current conjunction services and a separate model beyond ORDEM's validated region. Assess damage in a redundant, tensioned ribbon and inspect failure modes for a long moving line. A laptop render, ORDEM result alone or an ideal anchor score cannot confer deployment readiness. NASA ORDEM 3.2 user guide · NASA critical technology assessment.

8 Throughput and economic sensitivity

At one 1,000 kg gross departure per day with 500 kg of net cargo and 75% dispatch availability, theoretical delivery is 136,875 kg/year for one lane. At 7.46 days in transit, a daily dispatch schedule implies up to eight simultaneous ascending cars before descent, dwell or disabled-car contingencies. Cargo throughput and the number of loaded cars feed back into the dynamic load case. A transparent screening cost is C_net = (annualized capital + fixed annual cost)/net annual kg + variable cost per net kg. For illustrative inputs of $1 billion in fixed annual cost and the stated throughput, the fixed portion alone is $7,306/kg. At $0.10/kWh delivered electrical cost, the idealized 17.93 kWh per gross kg and 50% payload fraction imply about $3.59/kg of net cargo for ascent electricity. Both prices are scenario variables. The order-of-magnitude difference shows why duty cycle, payload fraction, capital, reliability and life matter more to modeled cost than the reversible mechanical work. Dispatch, terrestrial power prices and demand have not been forecast. These figures are unsuitable for an investment decision.

Commercial validation starts with orbital destinations and transfer interfaces, booking demand and realistic contingency windows. An elevator berth at GEO and conventional delivery to LEO are different services. Compare like destinations and insurance, schedule and loss assumptions before drawing economic conclusions. Near-term demonstrations could validate reusable inspection, tensile manufacturing and captive transport independently of closing the full orbital case.

9 Conclusions and reproducibility

A classical Earth elevator requires sustained, system-level specific tensile capacity and dynamic reliability at extreme scale. A taper of 20 needs 16.16 MJ/kg allowable in the bare model, above the best engineering product measurements demonstrated in this evidence set. Equatorial offshore geometry can be screened independently, with ports mapped as support facilities and rights and environmental constraints left to jurisdictional review. Linear electromagnetic motion is physically informative for a fixed terminal demonstration, and its distributed mass and alignment demands dominate the first-pass case for a full-length system. The pivotal next evidence is a measured, durable, joined ribbon with a defensible installed allowable and mass per meter over much longer gauges.

The companion package provides a standalone Python solver, input and output data, a complete GNoME metadata coverage report, screening source, site scoring, engineering evidence, and a native seven-scene Blender model with an assembly guide. The reference solver directly compares numerical quadrature against the closed-form potential, checks GEO and tip balance, and verifies integrated line loading. Catalog and siting packages preserve their source revisions or query windows. This study did not perform structural, orbital, environmental, contracting or regulatory certification.

References and data access

The source links in the text identify methods, manufacturer measurements and data extracts. Principal publications and data releases include the following.

- Pearson, J. (1975). The orbital tower: A spacecraft launcher using the Earth's rotational energy. Acta Astronautica 2(9–10), 785–799. Original paper.
- Edwards, B. C. (2000). Design and deployment of a space elevator. Acta Astronautica 47(10), 735–744. Original paper.
- Edwards, B. C. (2003). The Space Elevator. NASA Institute for Advanced Concepts Phase II final report. Technical report.
- Smitherman, D. V. Jr. (2005). Critical technologies for the development of future space elevator systems. International Astronautical Congress. NASA Technical Reports Server.
- Cohen, S. S. and Misra, A. K. (2009). The effect of climber transit on the space elevator dynamics. Acta Astronautica 64(5–6), 538–553. Original paper.
- Merchant, A. et al. (2023). Scaling deep learning for materials discovery. Nature 624, 80–85. Original paper · GNoME dataset documentation.
- Wang et al. (2026). Improvement of the tensile strength of carbon nanotube fibers to 12.5 GPa by fluidics-induced alignment and densification. Nature Communications 17, 8231. Original tensile study.
- Liu et al. (2026). Ultrahigh-ratio drawing during spinning achieves graphene fibres with high strength and thermal conductivity. Nature Materials 25, 1732–1740. Original tensile study.
- NASA Earth Observatory. Blue Marble Next Generation, July 2004 composite. Blender basemap imagery.